JOURNAL OF PROPULSION AND POWER
Vol. 10, No. 1, Jan.–Feb. 1994

Investigation of Shock/Turbulent Boundary-Layer Bleed Interactions

A. Hamed,* S. Shih,† and J. J. Yeuan†
University of Cincinnati, Cincinnati, Ohio 45221

A numerical investigation was conducted to determine the effect of bleed on oblique shock wave/turbulent boundary-layer interactions (SWBLI). The numerical solutions to the compressible Navier-Stokes equations reveal the flow details throughout the interaction zone and inside the normal bleed slot. Results are presented for an incident oblique shock of sufficient strength to cause boundary-layer separation on a flat plate in the absence of bleed at a freestream Mach number of 2.96 and Reynolds number of 1.2×10^7/ft, with bleed applied across the shock impingement location over a range of bleed mass flow rates corresponding to different values of plenum pressures. The results indicate a complex flow structure with large variations in both the normal and tangential flow velocities across the bleed slot. The flow entrainment into the slot is accompanied by an expansion-compression wave system with a bow shock originating inside the bleed slot. Increasing the bleed mass flow by decreasing the plenum pressure caused an initial decrease, then a later increase in the boundary-layer momentum and displacement thickness downstream of the interaction.

Introduction

THE control of flow separation in shock boundary-layer interactions can be accomplished through flow suction (bleed) in the interaction zone. In the case of mixed compression supersonic inlets, the bleed system design is critical to the efficient and stable operation of the system. Hamed and Shang[1] reviewed the existing experimental data for shock wave boundary-layer interactions in supersonic inlets and other related configurations. According to this survey, there is enough experimental evidence[2–7] to indicate that local bleed can control flow separation in shock wave/boundary-layer interactions. There are disagreements,[1] however, among the different experimental results regarding the effects of bleed location relative to the shock[2–4,7] and of bleed hole size.[7,8]

Strike and Rippy[2] obtained surface pressure measurements with porous bleed applied across and upstream of the shock impingement. Based on the minimum mass flow required for the static pressure downstream of the interaction to reach the theoretical pressure ratio, they determined that less suction is required when applied upstream. Seebough and Childs[3] who conducted their oblique shock wave boundary-layer bleed study over the inner surface of a cylinder, with a cone as a shock generator, concluded that across the shock bleed was more effective in controlling boundary-layer separation. Hingst and Tanji[4] and Benhachmi et al.[5] used pressure taps to measure the surface pressure, and hot wire to measure the bleed mass flow distribution through normal holes in SWBLI. Their results indicated that the bleed mass flow distribution followed the surface pressure distribution. In addition, Hingst and Tangi[4] used pitot probe surveys and surface flow visualization to compare the performance of bleed locations upstream, across, and downstream the shock. According to this study, across the shock and downstream bleed produced similar results in terms of removing flow separation, shortening the interaction length, increasing the pressure gradient, and producing fuller velocity profiles downstream of the interaction. Lee and Leblanc[6] presented their experimental results from taps, schlieren, pitot, and static probes for two levels of suction applied through porous wall sections across the shock impingement point. The poor performance of the weak suction was attributed to the effects of surface roughness.

Fukuda et al.[7] determined experimentally the change in boundary-layer characteristics across oblique shock wave interactions with bleed over the centerbody and cowl of a supersonic inlet. This study was conducted at different bleed mass flow rates, bleed hole sizes, bleed locations relative to the shock, and bleed hole inclination relative to the surface. Based on the change in boundary-layer displacement and momentum thicknesses, and in the transformed form factor for the different bleed configurations, they concluded that bleeding upstream and downstream of the interaction was preferable to bleeding across the shock. These results were unchanged by the normal bleed hole size which was found to have a negligible effect on the results.

Most viscous flow computations in supersonic inlets[9–15] require some knowledge of bleed flow rates and/or pressure distribution in the bleed regions. Comparisons of internal flow computational results with the experimental measurements in supersonic inlets revealed reasonable agreement between the computed and measured surface pressures upstream of the ramp bleed. However, discrepancies in the predicted shock locations and velocity profiles downstream of shock boundary-layer interactions with bleed suggest deficiencies in the bleed modeling. Other investigators actually solved the flow through the boundary layer and into the bleed slot, providing insight into the bleed flow region.[16,17] This approach eliminates the need for experimentally derived bleed models for supersonic inlet flow simulations, but can be very costly computationally.

Recently, some research efforts have been directed at improving bleed models. Paynter et al.[18] used the rough wall algebraic turbulence model of Cebeci and Chang[19] to simulate the overall effect of bleed on the growth of the boundary layer. The proper values of the roughness parameters were determined through matching the computational and test results for near wall velocity distributions downstream of the bleed band for seven bleed configurations, with shock boundary-layer interactions in some cases. The results of this in-

Presented as Paper 92-3085 at the AIAA/SAE/ASME/ASEE 28th Joint Propulsion Conference, Nashville, TN, July 6–8, 1992; received Aug. 20, 1992; revision received April 5, 1993; accepted for publication April 29, 1993.

*Professor, Department of Aerospace Engineering and Engineering Mechanics. Fellow AIAA.

†Department of Aerospace Engineering and Engineering Mechanics. Student Member AIAA.

vestigation demonstrate a strong dependence of the surface roughness on the fraction of the upstream boundary-layer mass flux removed. High roughness values were found for bleed rates between 3–15% of the upstream boundary-layer mass flux, but were insignificant for lower and higher bleed rates. Choked bleed flow through slanted holes gave the best boundary-layer profile in terms of flow separation control.

Hamed and Lehnig[20,21] conducted a numerical study in an incident oblique shock/laminar boundary-layer interaction, with bleed through a normal slot. By obtaining the flow solution in a domain that included the shock boundary-layer and extended inside the bleed slot, they were able to reveal the various regimes in this complex flowfield. Their results demonstrated a large variation in both the normal and tangential flow velocity distribution across the bleed slot opening at the plate surface. A separated flow region inside the bleed slot in the computed results suggests a reduction in the flow coefficient and total pressure. Hamed and Lehnig[21] presented the flowfields for three locations of the normal bleed slot, upstream, across, and downstream of the shock impingement point. The results demonstrated that for a given plenum pressure at the slot exit, the shock-induced flow separation on the plate was eliminated in the across the shock bleed configuration and reduced in the upstream and downstream bleed cases. Edwards and McRae[22] also computed the flowfield for an oblique incident shock, on a laminar boundary layer, with bleed through a normal slot across the shock impingement point. They compared the computed surface pressure distributions for a specified uniform normal bleed velocity across the slot to the plenum case, and demonstrated that the first case underpredicts the initial flow expansion into the slot. The solution domain for the plenum case was similar to that of Hamed and Lehnig,[20,21] but a uniform suction velocity was specified at the slot exit.

The discrepancies among the different experimental studies is an indication of the complexity of the flow in these configurations. Based on the comparison of their computational results with the experimental data of supersonic inlet flowfields, Reddy et al.[13] stressed the need for a detailed study of the effect of the individual bleed ports. Bleed optimization can only be accomplished through a parametric investigation in which the bleed conditions are changed systematically. The large number of parameters and the difficulties in obtaining accurate flow measurements in the interaction zone precludes a complete experimental investigation.

The purpose of the present study is to conduct a numerical investigation to characterize the flowfield in oblique shock wave/turbulent boundary-layer interactions with bleed, and to provide a basic understanding of the bleed flow controlling mechanisms. In the investigated configuration, flow suction (bleed) is applied through a normal slot located across the incident oblique shock on a flat plate turbulent boundary layer. The region inside the slot from the bleed surface to the plenum exit was included in the solution domain in order to realistically model the bleed flow and its variation with the plenum pressure. The results of the flow computations with different bleed mass flow rates reveal in detail the various flow regimes in the interaction region and within the bleed slot.

Computational Details

The PARC code[23] was used in the present investigation after conducting validation studies for shock wave/turbulent boundary-layer interactions,[24] with and without flow separation. The performance of four different codes with different turbulence models was assessed in terms of the agreement of their computed results with the experimental data of Refs. 25 and 26. The required grid refinement and computer time to reach this agreement were compared for incident shock on a flat plate boundary layer, and for flow over a compression corner. The prediction of the separation length, the surface pressure propagation upstream of the interaction, and the recovery of the skin friction downstream of the interaction received special attention. From the four assessed codes, the two[23,27] that use the implicit approximate factorization technique of Beam and Warming[28] to advance the solution, performed best both in terms of computer time and grid independence. Visbal's code[27] was the most robust, required the least number of time steps to reach convergence, and its computed results were consistently better than those obtained from the other codes with algebraic turbulence model. However, Avva et al.[29] proved the two equation k-ε model to be superior to the algebraic models for applications with separated flows. Consequently, the PARC code[23] was used in the present study because among the codes with the two equation turbulence models, it performed best, in terms of agreement with the experimental results and required the least grid refinement to achieve this agreement.[24] In addition, the PARC code was validated[30] through comparisons with experimental data for several flow configurations including supersonic flow over compression with separation, and has been used in several supersonic and hypersonic inlet flow simulations.[12–14,31]

Central differencing explicit and implicit dissipation schemes[32] are used in the PARC code for the solution of the Reynolds-averaged Navier-Stokes equations in strong conservation form. The Beam and Warming factorization algorithm coupled with Pulliam's pentadiagonal formulation form the basis of its implicit LU-ADI style solution scheme. The turbulence model used in the PARC code is based on Chien's low Reynolds number k-ε model[33] with Nichols[30] modifications to add com-

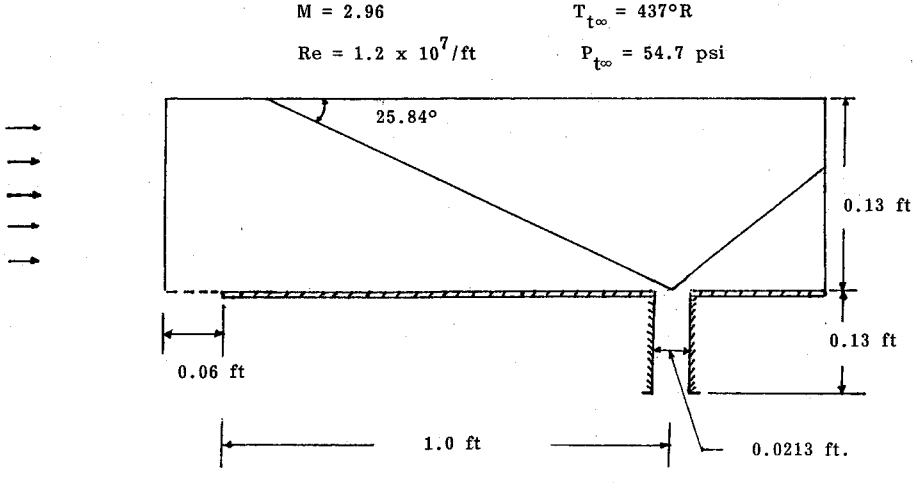

Fig. 1 Schematic of the solution domain.

pressibility effects. For the simulation, flow was considered to be turbulent throughout the calculation domain; no attempt was made to model transition and/or relaminarization.

Referring to Fig. 1, the solution domain used in the two-dimensional flow simulations extends upstream of the flat plate leading edge, downstream of the shock wave/turbulent boundary-layer interaction region, and inside the bleed slot, where the specified plenum pressure at the bottom controlled the amount of bleed mass flow. The incident oblique shock crosses the upper boundary, all other wave systems including the reflected, and any separation and reattachment shocks, cross the outflow boundary. Uniform freestream flow conditions are applied at the inflow boundary and all variables were extrapolated at the outflow boundary. No slip adiabatic flow conditions are applied at the plate and bleed walls. The static pressure is specified and first order extrapolation is applied for the rest of the flow variables at the bottom of the bleed slot. The location of the incident shock is fixed at the upper boundary with freestream and postshock conditions specified upstream and downstream. The slot was centered around the shock impingement location 1 ft from the flat plate leading edge. The grid spacing was varied in both x and y directions with clustering around both bleed walls and at the plate surface as shown in Fig. 2. The computational results were obtained with $\Delta y_{min} = \Delta x_{min} = 0.25794 \times 10^{-4}$ ft, corresponding to $y^+ = 2.0$ at $x = 0.9$ ft, using a 308/68 grid over the plate surface and a 75/68 grid inside the bleed slot, based on the grid refinement study results of Ref. 24. The computations for a typical bleed case required 5000 local time steps at 0.3 Courant-Friedrichs-Lewy (CFL) number to reach steady-state solution based on six orders of magnitude reductions in the averaged rms error in the flux.

Results and Discussion

The computations were performed at the incoming flow conditions of $M_\infty = 2.96$, $Re_\infty = 1.2 \times 10^7$/ft, $T_{t\infty} = 437°R$ and $P_{t\infty} = 54.7$ psi, and an impinging oblique shock angle of 25.84 deg. These are the same as the experimental test conditions of Law[25] for the separated flow case at a deflection angle δ of 7.93 deg. In his experimental study, Law used oil

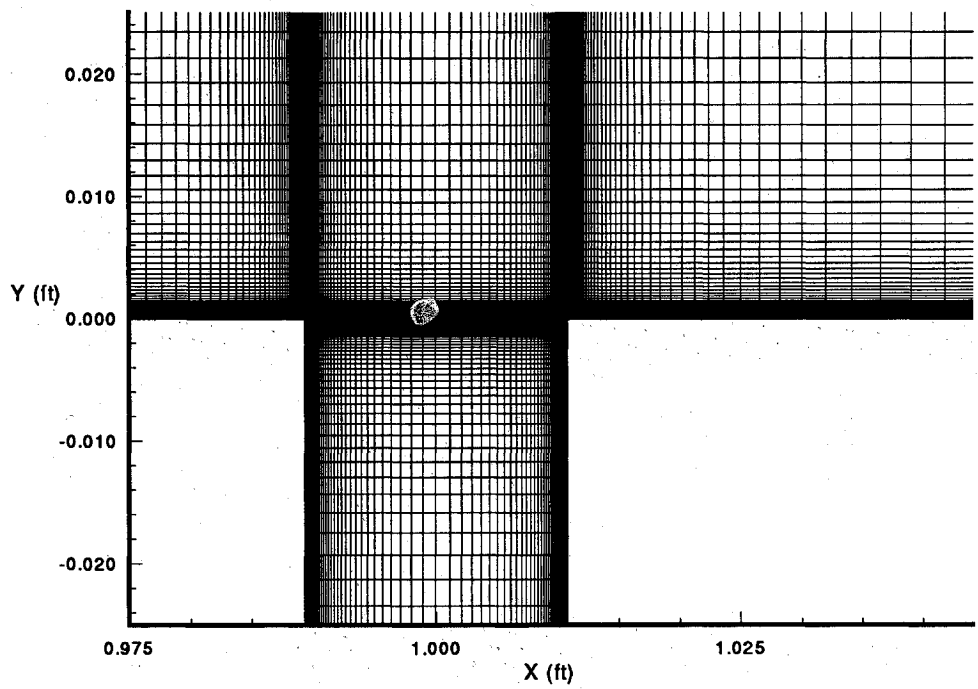

Fig. 2 Computational grid in the interaction region, bleed width = 0.0213 ft.

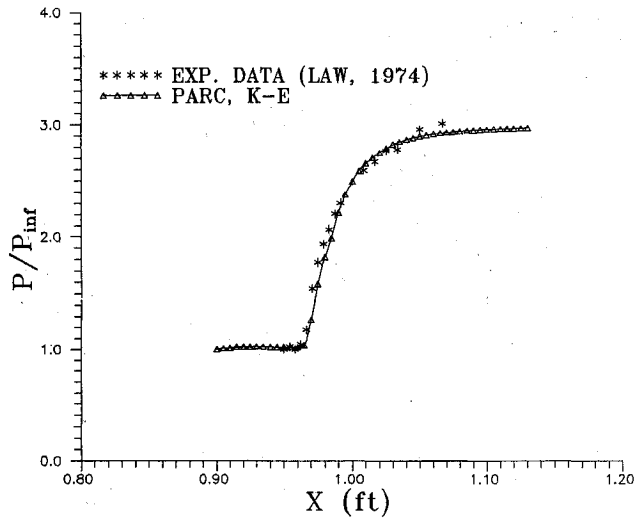

Fig. 3 Surface pressure distribution in the interaction region without bleed.

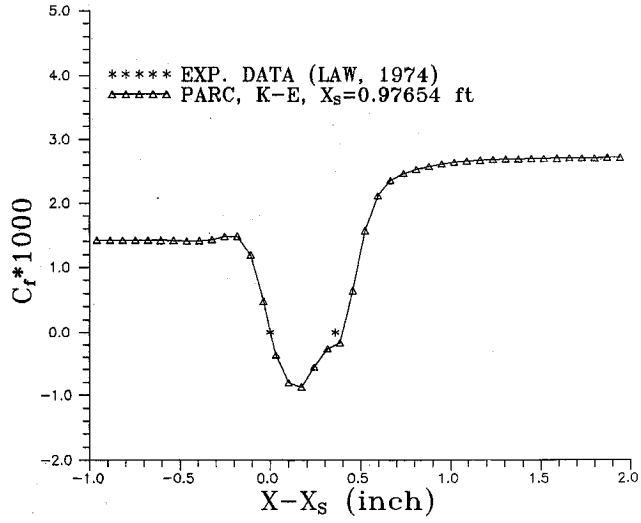

Fig. 4 Friction coefficient distribution in the interaction region without bleed. X_S = location of separation point.

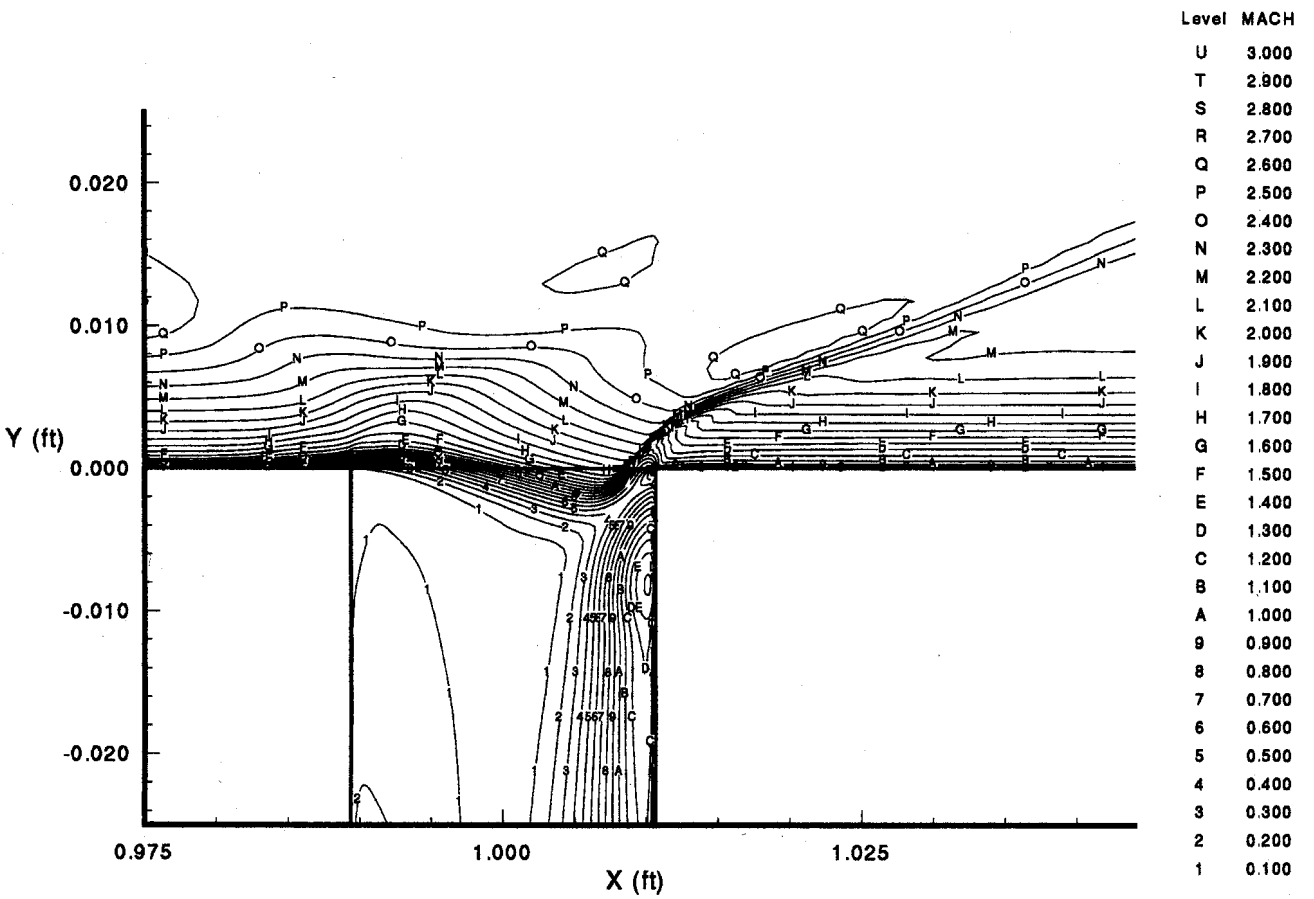

Fig. 5 Mach number contours, bleed width = 0.0213 ft, $P_b/P_{\text{inf}} = 1.5$.

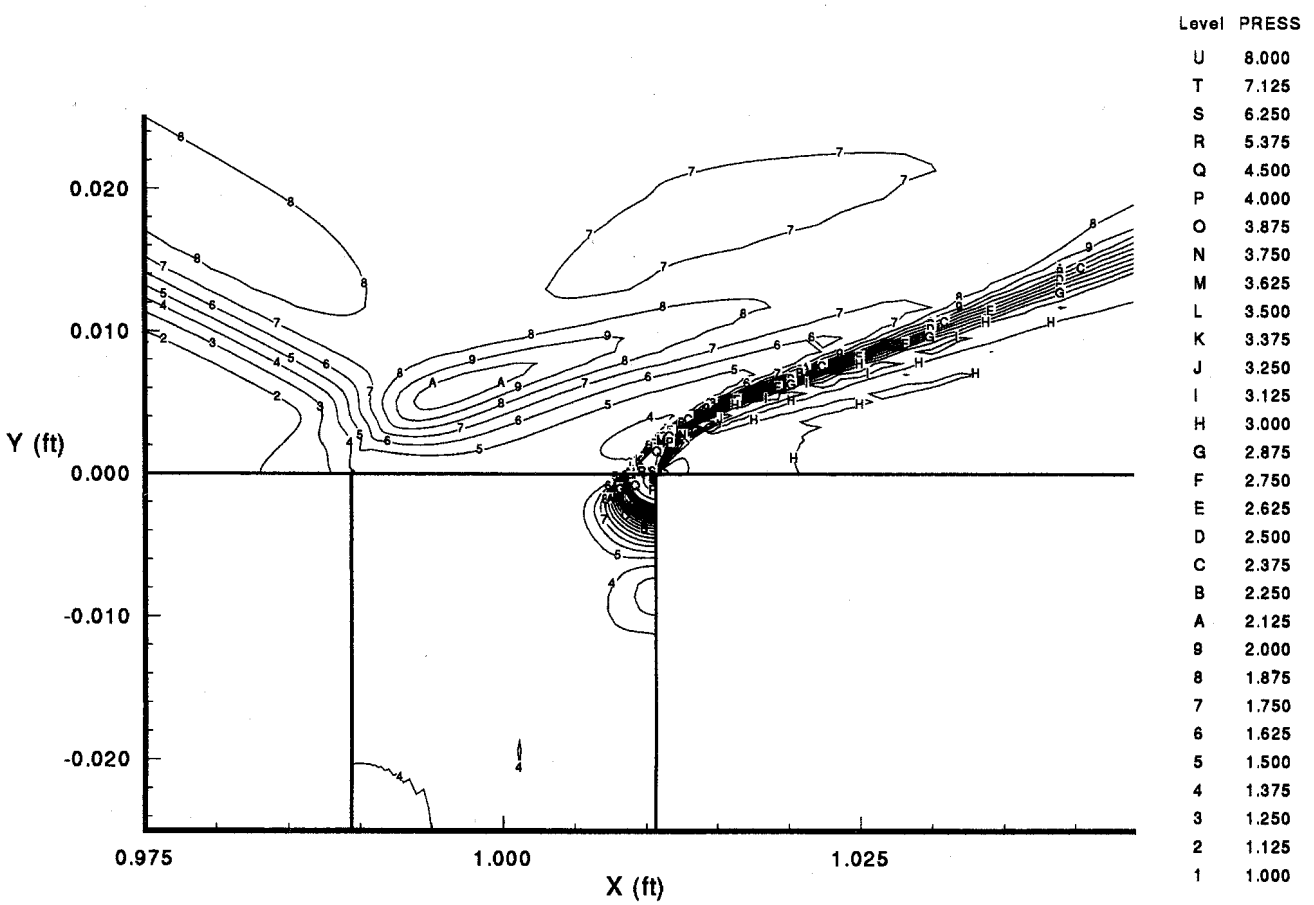

Fig. 6 Pressure contours, bleed width = 0.0213 ft, $P_b/P_{\text{inf}} = 1.5$.

flow visualization to reveal non-two-dimensional effects of the corner on the flat plate interior region. He measured the separation length for different shock generation spans and used these results to determine the proper reduced span to minimize the influence of the side wall interactions on the flat plate centerline. Figures 3 and 4 compare the computed surface pressure and skin friction without bleed to Law's centerline experimental data. One can see that the predicted separation length and surface pressure distribution are in very good agreement with the experimental results. The computations accurately predict the extent of the upstream influence of the shock boundary-layer interactions on the surface pressure and slightly overpredict the separation length.

The computations were performed under the same flow conditions with a bleed slot normal to the plate at different plenum pressure ratios ($0.95 \leq p_b/p_\infty \leq 1.95$). For an inviscid pressure ratio across the reflected shock p_2/p_∞ equals 2.962, and based on the downstream pressure p_2 the bleed plenum pressures are set to vary from choked to unchoked slot conditions ($0.321 < p_b/p_2 < 0.658$). The bleed slot width was 0.0213 ft, which is equal to 1.617 times the boundary-layer thickness upstream of the interaction at $x = 0.9$ ft. The details of the flowfield computational results near the bleed slot entrance are presented in Figs. 5–7 for a plenum pressure ratio of 1.5. They indicate a complex flow structure in which an expansion-compression system is associated with the flow entrainment into the slot opening. The initial flow turning is weak, then the flow is turned more strongly in the second

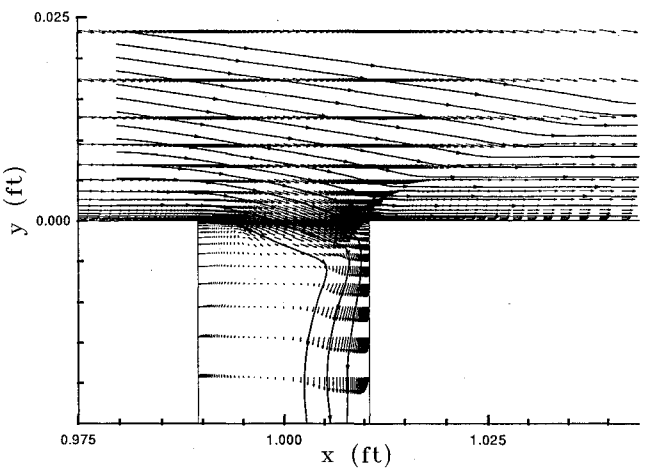

Fig. 7 Velocity fields and streamlines in the interaction region for bleed width = 0.0213 ft, P_b/P_{inf} = 1.5.

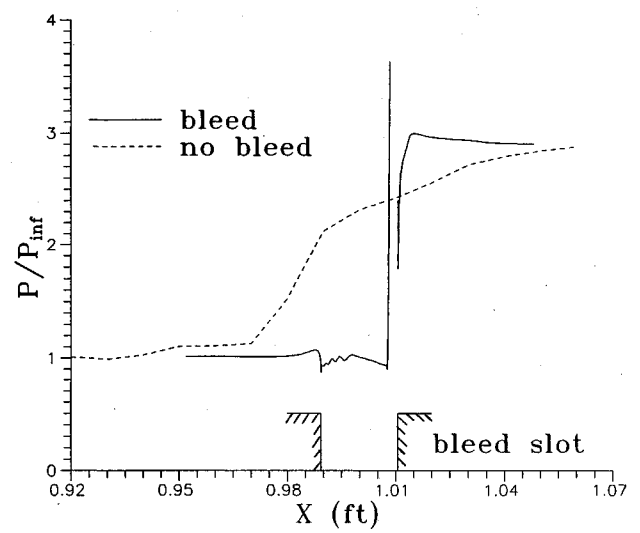

Fig. 8 Pressure distribution across the bleed opening for P_b/P_{inf} = 1.5.

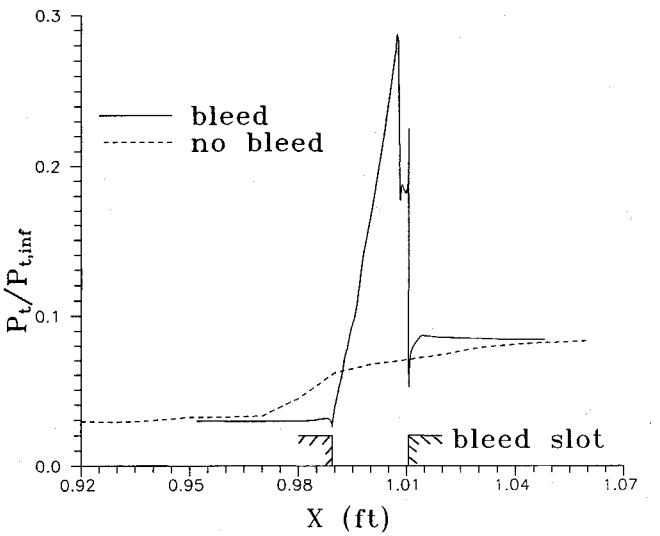

Fig. 9 Total pressure distribution across the bleed opening for P_b/P_{inf} = 1.5.

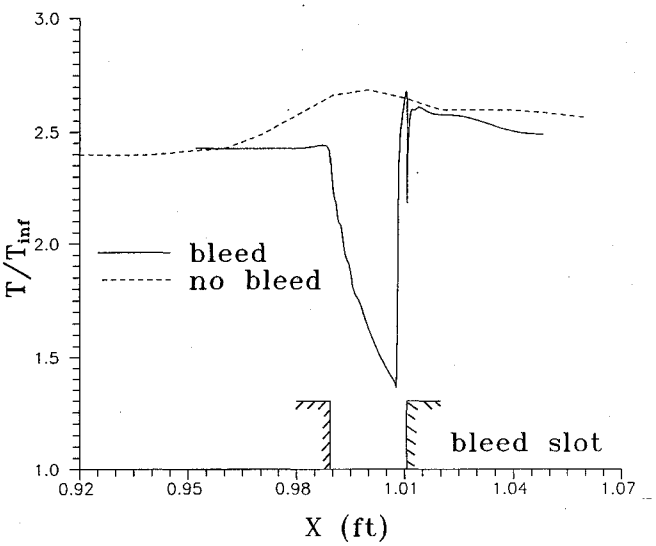

Fig. 10 Temperature distribution across the bleed opening for P_b/P_{inf} = 1.5.

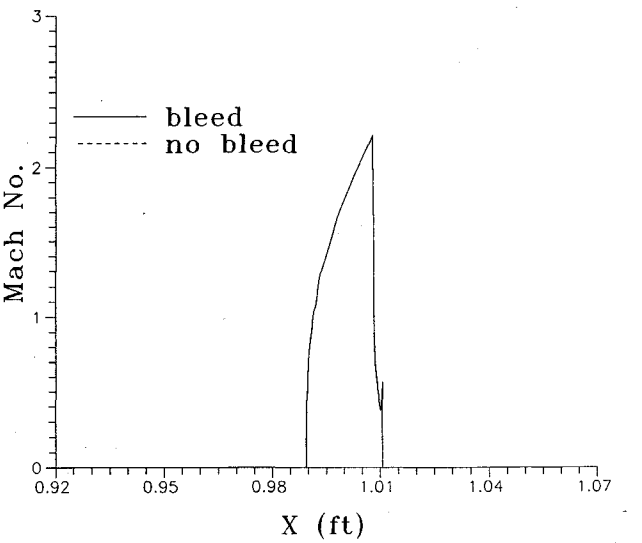

Fig. 11 Mach number distribution across the bleed opening for P_b/P_{inf} = 1.5.

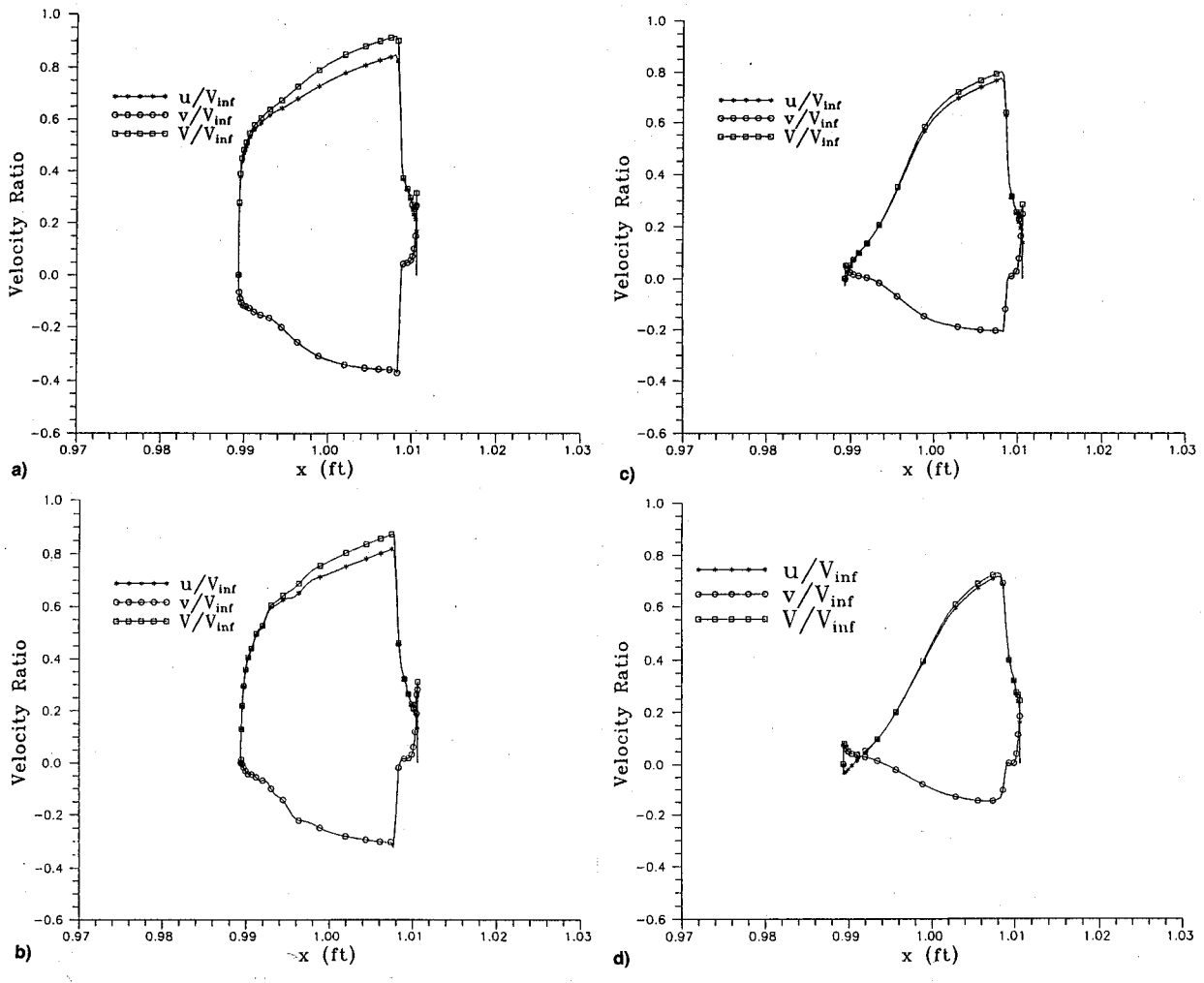

Fig. 12 Velocity distributions across the bleed opening for P_b/P_{inf} = a) 1.2, b) 1.5, c) 1.75, and d) 1.95.

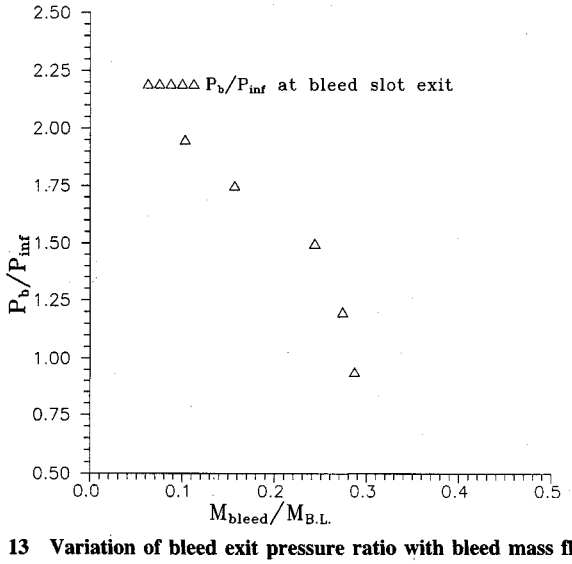

Fig. 13 Variation of bleed exit pressure ratio with bleed mass flow rate.

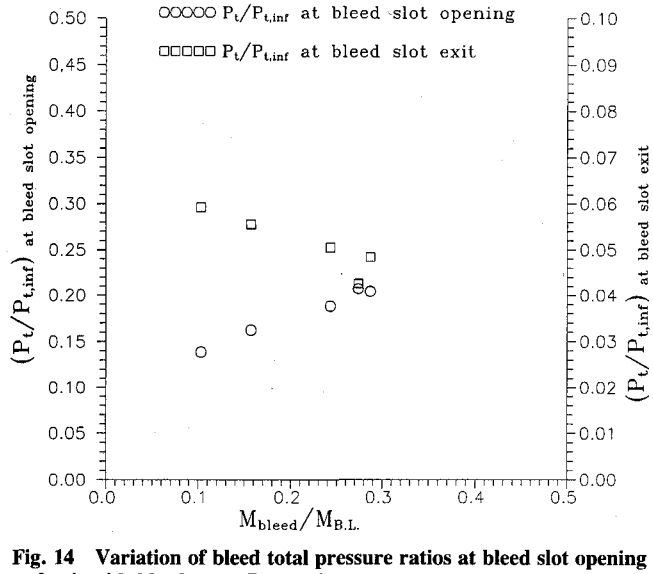

Fig. 14 Variation of bleed total pressure ratios at bleed slot opening and exit with bleed mass flow ratio.

half before crossing the bow shock that originates inside the slot. The Mach number contours show a stagnation point behind the bow shock near the plate corner, followed by an expansion fan. The flow inside the bleed slot is mostly confined to a strip adjacent to the back wall of the bleed slot, where the flow velocities reach supersonic values. A flow recirculation zone much larger than the laminar case[21] occupies most of the bleed slot. The computational results at different plenum pressure settings show that the dual separation and reattachment shock system is replaced by a single reflected shock structure, indicating no flow separation, for plenum pressure ratios ≤ 1.5. The corresponding variations in static and total pressures, static temperature, and Mach number across the bleed slot are presented in Figs. 8–11. These figures show the sudden change in the flow properties across the bow shock. One can observe a reduction in both the static and total pressure over the plate surface upstream

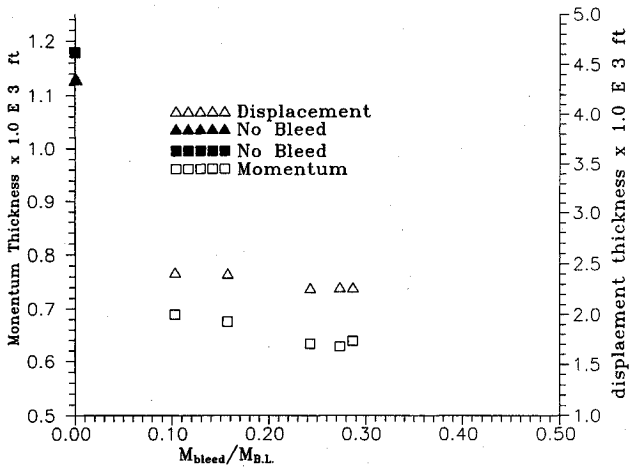

Fig. 15 Variation of displacement and momentum thickness downstream of the interaction at x = 1.13 ft with bleed mass flow rate.

of the slot opening due to the flow entrainment into the slot. Downstream of the slot opening, both the static and total pressure increase more sharply compared to the no bleed case.

Figure 12 presents the velocity distribution across of the bleed slot opening for different bleed flow rates. Large variations in both the normal and tangential velocity components can be seen across the slot opening with some mass injection near the upstream corner at the high-pressure plenum settings. The tangential velocity reaches values as high as 90% of the freestream velocity before dropping sharply behind the bow shock near the back wall.

The variations in the static pressure at the bleed slot exit with the calculated bleed mass flow are presented in Fig. 13. The corresponding changes in the mass averaged total pressure at the bleed slot inlet and exit are presented in Fig. 14. In these figures, the bleed mass flow is normalized with respect to the mass flow in the incoming boundary layer at x = 0.9, and the static and total pressures are normalized with respect to the freestream values. With the static pressure nearly constant across the bleed slot opening, except for the

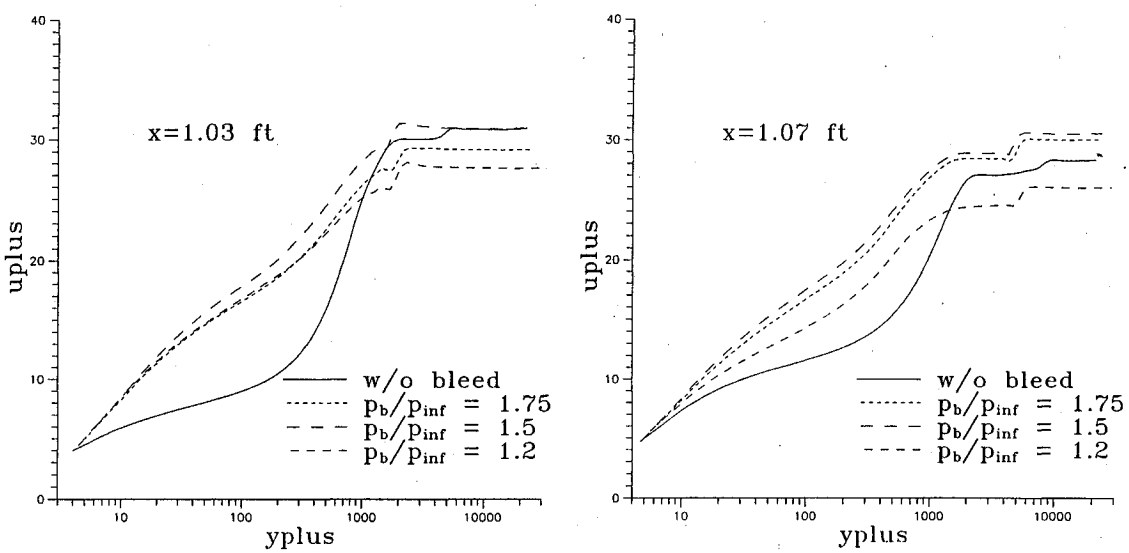

Fig. 16 Near wall velocity profiles downstream of the interaction at different bleed pressure ratios.

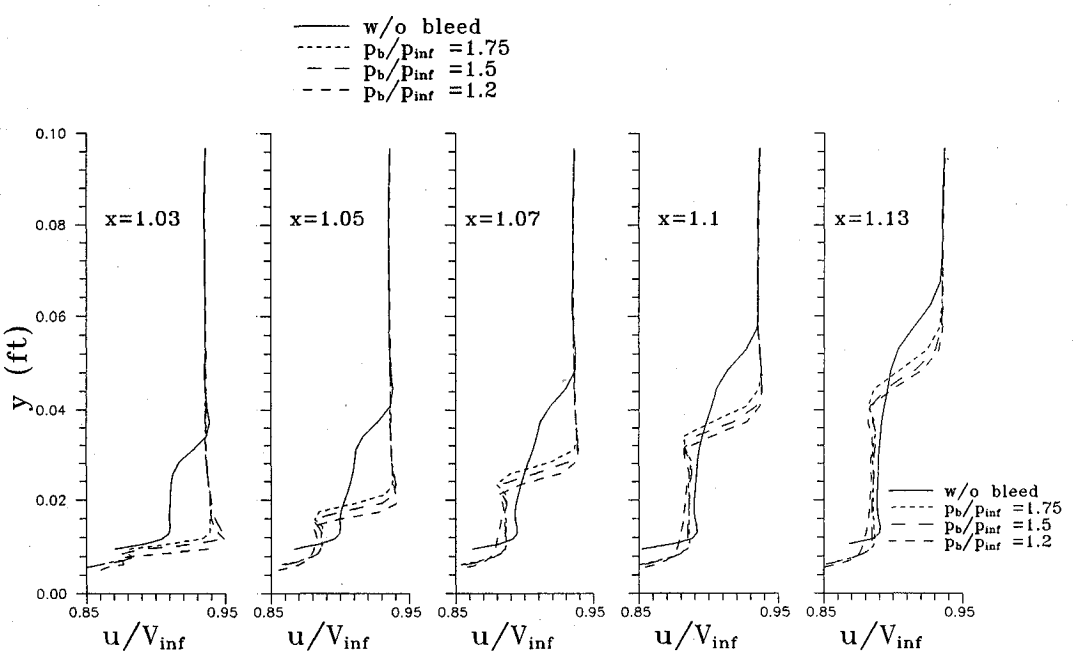

Fig. 17 Velocity profiles downstream of the interaction at different bleed pressure ratios.

sudden rise across the bow shock, the total pressure increase across the bleed slot opening is mainly associated with the increased flow velocities as the bleed mass flow increases. However, at the slot exit, the mass averaged total pressure is mostly influenced by the value of the static pressure due to the greater effects of the flow recirculation before choking. The corresponding variation in the boundary-layer displacement and momentum thickness are presented in Fig. 15. The results indicate that the boundary-layer displacement and momentum thicknesses downstream of the interaction initially decrease, then slightly increase with the increase in the bleed mass flow. According to Fig. 15, the maximum reduction in the boundary-layer displacement and momentum thickness downstream of the interaction are achieved at plenum pressure ratios of 1.2 and 1.5, respectively. The corresponding bleed mass flows are 27.38 and 24.31% of the incoming boundary-layer mass flow upstream of the interaction.

The near wall velocity profiles downstream of the interaction are presented in Fig. 16 for three cases with plenum pressure ratios of 1.2, 1.5, and 1.75. This figure shows that the velocities near the wall are higher for the case $p/p_\infty = 1.5$ than for both higher and lower bleed mass flow cases, $p/p_\infty = 1.2$ and $p/p_\infty = 1.75$. This can be attributed to the balance between the increases in the flow velocities and bow shock strength with the increased bleed mass flow. Figure 17 shows the variation in the flow velocity profiles downstream of the interaction outside the boundary layer for the three bleed cases corresponding to plenum pressure ratios of 1.2, 1.5, and 1.75 and for the no bleed case. This figure illustrates the reflected shock structure, with the strong bow shock closest to the wall, followed by the expansion fan, then the weaker separation shock further out. Figure 17 shows that as the bleed mass flow increases, the reflected shock system moves closer to the wall.

Conclusions

The objective of this work was to provide a basic understanding of the flow in the shock boundary-layer interactions and of the mechanisms for its control. Numerical computations were conducted in oblique shock wave/turbulent boundary-layer interaction to reveal in details the flow characteristics, and how they are altered by bleed. Flow suction (bleed) was accomplished through a normal slot across the shock incident point. The bleed results reveal a complex flow structure in the interaction zone and inside the bleed slot. The flow accelerates across the top of the bleed port, crosses a bow shock formed near the downstream corner, then goes through an expansion fan at the corner. A large recirculation region dominates the flow inside the bleed slot, and the bleed mass flow is limited to a narrow region adjacent to the downstream bleed wall, where the velocity reaches supersonic values. The effect of the bleed mass flow rate was investigated by changing the specified plenum pressure at the bottom of the slot and comparing the boundary-layer characteristics downstream of the interaction. As the bleed mass flow increased, the boundary-layer momentum and displacement thickness initially decreased, then slightly increased downstream of the interaction. In terms of the boundary-layer characteristics downstream of the interaction, the best performance was obtained when 24–27% of the boundary-layer mass flow upstream of the interaction was removed.

Acknowledgments

This work was sponsored by Air Force Office of Scientific Research Contract 91-0101, L. Sakell, Project Monitor; and by NASA Grant NAG3-1213, Dave Saunders, Project Monitor. The authors would like to acknowledge the invaluable discussions of Bob Coltrin of NASA Lewis Research Center. The computational work was performed on the CRAY YMP of the Ohio Supercomputer.

References

[1]Hamed, A., and Shang, J., "Survey of Validation Data Base for Shock Wave Boundary-Layer Interactions in Supersonic Inlets," *Journal of Propulsion and Power*, Vol. 7, No. 4, 1991, pp. 617–625.

[2]Strike, W. T., and Rippy, J., "Influence of Suction on the Interaction of an Oblique Shock with a Turbulent Boundary Layer at Mach 3," Arnold Engineering Development Center TN-61-129, Oct. 1961.

[3]Seebaugh, W., and Childs, M., "Conical Shock Wave Boundary-Layer Interaction Including Suction Effects," *Journal of Aircraft*, Vol. 7, No. 4, 1970, pp. 334–340.

[4]Hingst, W. R., and Tanji, F. T., "Experimental Investigation of Two-Dimensional Shock-Boundary Layer Interaction with Bleed," AIAA Paper 83-0135, Jan. 1983; see also NASA TM-83057, Jan. 1983.

[5]Benhachmi, D., Greber, I., and Hingst, W., "Experimental and Numerical Investigation of an Oblique Shock-Wave/Turbulent Boundary Layer Interaction with Continuous Suction," AIAA Paper 89-0357, Jan. 1989.

[6]Lee, D. B., and Leblanc, R., "Interaction onde de Choc Oblique-Couche Limite sur Paroi Poreuse avec Aspiration," Improvement of Aerodynamic Performance Through Boundary Layer Control and High Lift Systems, Paper 23, AGARD CP-365, Aug. 1984.

[7]Fukuda, M. K., Hingst, W. R., and Reshotko, E., "Bleed Effects on Shock/Boundary-Layer Interactions in Supersonic Mixed Compression Inlets," *Journal of Aircraft*, Vol. 14, No. 2, 1977, pp. 151–156.

[8]Wong, W. F., "The Application of Boundary Layer Suction to Suppress Strong Shock-Induced Separation in Supersonic Inlets," AIAA Paper 74-1063, Oct. 1974.

[9]Hunter, L. G., Tripp, J. M., and Howlett, D. G., "A Mach 2.0 Plus Supersonic Inlet Study Using the Navier-Stokes Equations," AIAA Paper 85-1211, July 1985.

[10]Chyu, W. J., Kawamara, T., and Bencz, D. P., "Navier-Stokes Solutions for Mixed Compression Axisymmetric Inlet Flow with Terminal Shock," *Journal of Propulsion and Power*, Vol. 5, No. 1, 1989, pp. 4, 5.

[11]Shigematsu, J., Yamamoto, K., and Shiraishi, K., "Numerical Investigation of Supersonic Inlet Using Implicit TVD Scheme," AIAA Paper 90-2155, July 1990.

[12]Weir, L. J., Reddy, D. R., and Rupp, G. D., "Mach 5 Inlet CFD and Experimental Results," AIAA Paper 89-2355, July 1989.

[13]Reddy, D. R., Benson, T. J., and Weir, L. J., "Comparison of 3-D Viscous Flow Computations of Mach 5 Inlet with Experimental Data," AIAA Paper 90-0600, Jan. 1990.

[14]Saunders, J. D., and Keith, T. G., Jr., "Results from Computational Analysis of a Mixed Compression Supersonic Inlet," AIAA Paper 91-2581, June 1991.

[15]Rizzetta, D. P., "Numerical Simulation of a Supersonic Inlet," AIAA Paper 91-0128, Jan. 1991.

[16]Forester, C. K., and Tjonneland, E., "New Guide for Accurate Navier-Stokes Solution of Two-Dimensional External Compression Inlet with Bleed," International Council of the Aeronautical Sciences 88-2.5.1, 1988.

[17]Fujimoto, A., Niwa, N., and Sawada, K., "Numerical Investigation on Supersonic Inlet with Realistic Bleed and Bypass Systems," AIAA Paper 91-0127, Jan. 1991.

[18]Paynter, G. C., Treiber, D. A., and Knelling, W. D., "Modeling Supersonic Inlet Boundary Layer Bleed Roughness," AIAA Paper 92-0269, Jan. 1992.

[19]Cebeci, T., and Chang, K. C., "Calculation of Incompressible Rough-Wall Boundary Layer Flows," *AIAA Journal*, Vol. 16, No. 7, 1978, pp. 730, 731.

[20]Hamed, A., and Lehnig, T., "An Investigation of Oblique Shock/Boundary Layer/Bleed Interaction," *Journal of Propulsion and Power*, Vol. 8, No. 2, 1992, pp. 418–424.

[21]Hamed, A., and Lehnig, T., "The Effect of Bleed Configuration on Shock/Boundary Layer Interactions," AIAA Paper 91-2014, June 1991.

[22]Edwards, J., and McRae, D., "Solution Technique for Shock-wave-Boundary Layer Interactions with Flow Separation and Slot Suction Effects," AIAA Paper 91-0652, Jan. 1991.

[23]Cooper, G. K., and Sirbaugh, J. R., "PARC Code: Theory and Usage," Arnold Engineering Development Center TR-89-15, Dec. 1989.

[24]Hamed, A., "An Investigation of Oblique Shock/Boundary Layer Interaction Control," Univ. of Cincinnati, Dept. of Aerospace Engineering and Engineering Mechanics, Air Force Office of Scientific Research Annual Rept. 101, Cincinnati, OH, Jan. 24, 1992.

[25]Law, C. H., "Supersonic Turbulent Boundary-Layer Separation," *AIAA Journal*, Vol. 12, No. 6, 1974, pp. 794–797.

[26]Settles, G. S., Fitzpatrick, P. J., and Bogdonoff, S. M., "Detailed Study of Attached and Separated Compression Corner Flowfields in High Reynolds Number Supersonic Flow," *AIAA Journal*, Vol. 17, No. 6, 1979, pp. 579–585.

[27]Visbal, M., "Calculation of Viscous Transonic Flows About a Supercritical Airfoils," Air Force Wright Aeronautical Labs. TR-86-3013, July 1986.

[28]Beam, R., and Warming, R. F., "An Implicit Factored Scheme for the Compressible Navier-Stokes Equations," *AIAA Journal*, Vol. 16, No. 4, 1978, pp. 393–402.

[29]Avva, R., Smith, C., and Singal, A., "Comparative Study of High and Low Reynolds Number Versions of k-ε Models," AIAA Paper 90-0246, Jan. 1990.

[30]Nichols, R. H., "A Two-Equation Model for Compressible Flows," AIAA Paper 90-0494, Jan. 1990.

[31]Reddy, D. R., Smith, G. E., and Liou, M. F., "Three-Dimensional Viscous Analysis of a Hypersonic Inlet," AIAA Paper 89-0004, Jan. 1989.

[32]Jameson, A., Schmidt, W., and Turkel, E., "Numerical Solutions of the Euler Equations by Finite Volume Methods Using Runge-Kutta Time-Stepping Schemes," AIAA Paper 81-1259, 1981.

[33]Chien, K.-Y., "Prediction of Channel and Boundary-Layer Flows with a Low Reynolds Number Turbulence Model," *AIAA Journal*, Vol. 20, No. 1, 1982, pp. 33–38.